Accepted Manuscript

Modulation of the molecular arrangement in artificial and biological membranes by phospholipid-shelled microbubbles

Dario Carugo, Miles Aron, Erdinc Sezgin, Jorge Bernardino de la Serna, Marina Kuimova, Christian Eggeling, Eleanor Stride

PII: S0142-9612(16)30585-3

DOI: 10.1016/j.biomaterials.2016.10.034

Reference: JBMT 17771

To appear in: *Biomaterials*

Received Date: 26 August 2016

Revised Date: 22 October 2016

Accepted Date: 23 October 2016

Please cite this article as: Carugo D, Aron M, Sezgin E, Bernardino de la Serna J, Kuimova M, Eggeling C, Stride E, Modulation of the molecular arrangement in artificial and biological membranes by phospholipid-shelled microbubbles, *Biomaterials* (2016), doi: 10.1016/j.biomaterials.2016.10.034.

Modulation of the molecular arrangement in artificial and biological membranes by phospholipid-shelled microbubbles

Dario Carugo[a†*], Miles Aron[a†], Erdinc Sezgin[b], Jorge Bernardino de la Serna[b,c], Marina Kuimova[d], Christian Eggeling[b], and Eleanor Stride[a]**

[a] Institute of Biomedical Engineering, Department of Engineering Science, University of Oxford, Oxford OX3 7DQ, United Kingdom; [b]MRC Human Immunology Unit, Weatherall Institute of Molecular Medicine, University of Oxford, Headley Way, Oxford OX3 9DS, United Kingdom; [c]Research Complex at Harwell, Central Laser Facility, Rutherford Appleton Laboratory, Science and Technology Facilities Council, Harwell-Oxford OX11 0FA, United Kingdom; [d]Department of Chemistry, Imperial College London, London SW7 2AZ, United Kingdom;

Abstract

The transfer of material from phospholipid-coated microbubbles to cell membranes has been hypothesized to play a role in ultrasound-mediated drug delivery. In this study, we employed quantitative fluorescence microscopy techniques to investigate this phenomenon in both artificial and biological membrane bilayers in an acoustofluidic system. The results of the present study provide strong evidence for the transfer of material from microbubble coatings into cell membranes. Our results indicate that transfer of phospholipids alters the organization of molecules in cell membranes, specifically the lipid ordering or packing, which is known to be a key determinant of membrane mechanical properties, protein dynamics, and permeability. We further show that polyethylene-glycol, used in many clinical microbubble formulations, also has a major impact on both membrane lipid ordering and the extent of lipid transfer, and that this occurs even in the absence of ultrasound exposure.

Keywords: Microbubbles; Ultrasound; Lipid order; Membrane bilayers

Short title: Microbubble Mediated Membrane Modulation

[*] Corresponding author: Prof. Eleanor Stride, Institute of Biomedical Engineering, Department of Engineering Science, University of Oxford, Oxford OX3 7DQ, United Kingdom. Email: Eleanor.stride@eng.ox.ac.uk; fax: +44(0)1865 617 728

[**] Current address: Faculty of Engineering and the Environment, Engineering Sciences Academic Unit, University of Southampton, Southampton SO17 1BJ, United Kingdom

[†] Authors have equally contributed to the work in this study.

1. Introduction

Gas-filled microbubbles (MBs) stabilized by a surfactant or polymer coating are routinely used in medical imaging as ultrasound (US) contrast agents, capable of enhancing US backscatter from blood by several orders of magnitude [1]. The MB core typically consists of a high molecular weight gas (e.g., perfluorocarbon or sulphur hexafluoride) to enhance sample stability both *in vivo* and during handling or storage. The outer coating may consist of a cross-linked protein, saturated phospholipid or lipid mixture. Composition strongly influences MB acoustic response and hence clinical utility [2]. Polyethylene glycol (PEG) chains covalently bonded to either phospholipids or fatty acids can also be integrated into the coating in order to reduce immunogenicity [3, 4], and PEG has furthermore been reported to influence the physical characteristics of the end-product in MB production processes [3, 5].

The surfactant coating can be employed as a scaffold for the attachment of biologically active compounds [6] and/or targeting agents [7]. This has paved the way for the use of MBs as vehicles in therapeutic applications such as drug delivery and/or gene therapy [8-10] [2]. Their responsiveness to US facilitates triggered release of the therapeutic material; and, even more importantly, the interaction between MBs and living cells in an US field has been observed to generate cell membrane permeabilization, through a process often referred to as 'sonoporation' [11]. Although the underlying mechanisms have not been clearly identified, it has been postulated that the mechanical action of US-activated MBs causes the formation of temporary pores within nearby cellular membranes [6], which can be exploited to effectively deliver compounds into the intracellular milieu. Pore formation has been revealed and characterized *in vitro* using confocal microscopy [11], membrane potential measurements [12] and scanning and transmission electron microscopy [13]. In some cases, however, pores do not reseal spontaneously and this can lead to cell death [11, 14-16].

The mechanical perturbation of the cellular microenvironment during US exposure in the presence of MBs may be attributed to distinct physical phenomena, including the pushing-and-pulling effect of a volumetrically oscillating MB [17, 18], acoustic radiation forces causing MB translation against or across the cell membrane [19, 20], fluid shear stress fields generated by acoustic microstreaming [21], or shock waves and fluid jets produced by MB collapse [11, 22]. Mechanistic studies have been conducted to investigate the mechanical interaction between US-activated MBs and either artificial [23] or biological membrane bilayers [18]. Giant unilamellar vesicles (GUVs) composed of unsaturated phospholipids were observed to undergo elongational or compressional deformation when approaching or receding from a MB respectively, under low-pressure US fields [17, 23]. At sufficiently high shear rates and/or elongation amplitudes pore formation occurred, which was accompanied by vesicle rupture [23]. Importantly, the deformation and break-up dynamics of GUVs have been observed to depend on the mechanical properties of the membrane bilayer [24]. Cyclic elongational and compressional membrane deformation have also been observed on adherent cells *in vitro* [17], and a direct

correlation between cell membrane strain and the resulting transient permeabilization has been demonstrated using fluorescent probes [17].

Alternative mechanisms have also been suggested to govern or enhance US-mediated intracellular delivery, including: (i) activation of clathrin-mediated endocytic pathways [2, 19, 25], (ii) alteration of reactive oxygen species (ROS) homeostasis [26] potentially due to increased intracellular H_2O_2 levels [27], (iii) influx of calcium ions (Ca^{2+}) [12], and (iv) potential exchange or fusion of the phospholipid MB shell with the phospholipid bilayer of a cell membrane [28-30]. In recent years significant efforts have been made to characterize the behaviour of biological membranes exposed to US-activated MBs and to identify the underlying interaction phenomena [31], particularly regarding membrane permeabilization and recovery dynamics [11, 32]. Nevertheless, the lack of quantitative methods for investigating the biophysical perturbations at a sub-cellular level often impedes correlation of experimental observations with biochemical or biophysical events.

In the present study we employed acoustofluidic systems integrated with quantitative fluorescence microscopy techniques to measure changes in the physical properties of both artificial and biological membrane bilayers interacting with phospholipid-shelled MBs, both in the presence and absence of an US field. We have focused primarily on changes in the arrangement of membrane lipids, given the latter's relevance to a variety of biophysical properties and membrane-associated cellular processes, including mobility, function and organization of membrane proteins [33, 34], formation and dynamics of membrane domains [35], membrane mechanical properties [36] and permeability [37].

2. Materials and Methods

2.1 Methods rationale

In order to investigate the effect of US and/or MBs of different composition in model and cell membranes we studied several biophysical characteristics that indicate how tightly lipids are packed within the membrane, namely: membrane viscosity, lipid order and lipid mobility.

Initially we investigated material transfer from MBs to live-cell membranes using a fluorescent, lipid-mimetic membrane probe. Next, to investigate changes in biophysical membrane properties after transfer, we selected giant unilamellar vesicles (GUVs) as a membrane model [38]. GUVs composed of dioleoyl phosphatidylcholine (DOPC) were specifically employed, since the resultant membrane model was a highly disordered system in terms of lipid arrangement, in contrast to the well ordered lipid shell typical of MBs. In this way, we were able to maximise the sensitivity of our model system in order to verify the ability of microscopy-based techniques to quantify changes in membrane physical properties. Multiple techniques including fluorescence lifetime measurement of a viscosity-sensitive membrane probe, membrane order characterisation using spectral imaging with an environmentally sensitive probe, and lipid mobility using fluorescence-

correlation-spectroscopy (FCS) on a fluorescent lipid analogue were employed to validate the biophysical membrane characteristics. Increased lipid order was found to be associated with reduced diffusion time and increased membrane viscosity in agreement with previous studies [39].

In view of these results, we opted for using spectral imaging in living cells, as a means to efficiently measure changes in lipid order over statistically significant numbers of cell membranes. This approach was preferred to point-measurements (i.e., FCS) or more laborious techniques, to allow for analysis of large data samples. In these experiments, we further characterised dependencies on MB formulation. For this reason, MBs were produced in-house so as to be able to control and vary their composition.

Ultrasound exposure was performed using an acoustofluidic device developed in house for integration with advanced microscopy techniques. The device was designed to operate at a frequency of ~1MHz, which is an ultrasound frequency employed in many studies investigating ultrasound-mediated drug delivery [19]. The acoustic amplitude was selected to be sufficiently high to cause cavitation microstreaming, but low enough to avoid an undesirable increase in fluid temperature.

2.2 Formation of giant unilamellar vesicles (GUVs)

GUVs made of DOPC (from Avanti Polar Lipids, USA) were employed as cell models and produced by electroformation as initially proposed by Angelova et al. [40], but following a modified version of the original protocol [41]. Briefly, a custom built Teflon® electroformation chamber containing two platinum (Pt) wires parallel to each other was employed. The lipid solution (1 mg/mL in chloroform) was spread on the Pt wires (3 μL per wire) and left at room temperature for 2 h for the solvent to evaporate. The electroformation chamber was primed with approximately 350 mL of a sucrose solution (300 mM in deionized water), and the Pt wires were connected to a signal generator. A sinusoidal wave was generated at 2V RMS and 10 Hz for approximately 1.5 h, which resulted in GUVs formation over the wires surface. The signal frequency was subsequently reduced down to 2 Hz for approximately 20 min, allowing the GUVs to detach from the wires. The formed GUVs were removed from the chamber using a micropipette, and transferred to a chambered (8-well) coverslip for labelling (µ-Slide 8 Well, Ibidi GmbH, Germany). The GUV concentration in the final sample was equal to ~1×10^4 GUVs/mL.

2.3 Preparation and characterisation of microbubble suspensions

A phospholipid-coated MB formulation frequently employed in therapeutic applications consisting of 1,2-Distearoyl-sn-glycero-3-phosphocholine (DSPC, Avanti Polar Lipids, USA) and polyoxyethylene (40) stearate (PEG40S, Sigma Aldrich, UK) in a 9:1 molar ratio was selected as the primary MB model in the present study [42, 43]. Additional MB formulations investigated include DSPC-PEG40S MB with a 90:1 molar ratio, DSPC MB with no PEG40S, and 1,2-dibehenoyl-sn-glycero-3-phosphocholine (DBPC, Avanti Polar Lipids, USA) MB with no PEG40S.

All MBs were produced using a previously reported batch sonication protocol [44]. Briefly, 1,2-Distearoyl-sn-glycero-3-phosphocholine (DSPC, Avanti Polar Lipids, USA) and polyoxyethylene (40) stearate (PEG40S, Sigma Aldrich, UK) were dissolved in chloroform (Sigma Aldrich, UK) and mixed in a glass vial at either a molar ratio of 9:1 (total volume = 1.1 mL) or 90:1 (total volume = 0.67 mL). The mixture was subsequently heated on a hotplate set to 50ºC for 12 h, to allow for the solvent to evaporate. The obtained dry lipid film was suspended in 5 mL of phosphate buffered saline (PBS, pH 7.4) solution (Thermo Fisher Scientific Inc., USA) for 1 h on a hotplate set at 100ºC. Lipids were then homogeneously dispersed for 150 s using a sonicator (XL 2000, probe diameter 3 mm, 20 W, 22.5 kHz, Misonix, USA) at a power setting of 3 with the tip completely immersed in the lipid solution. MBs were subsequently formed by placing the sonicator tip at the air-water interface under constant sulphur hexafluoride flow (The BOC Group plc, UK) and sonicating for 30 sec at a power setting of 14. Immediately after production, the vial containing the MB suspension was capped and placed in ice for approximately 5 min.

In those experiments looking at the effect of DSPC only on the physical properties of cell membranes, MBs made of pure DSPC were produced using the same protocol reported previously. For this purpose, the starting lipid solution consisted of 0.62 mL of DSPC dissolved in chloroform at a concentration of 25 mg/mL. In our experience, these microbubbles form more reliably by reducing the temperature prior to the final sonication step to 60°C. For those experiments using MBs made of pure 1,2-dibehenoyl-sn-glycero-3-phosphocholine (DBPC, Avanti Polar Lipids, USA), MBs were produced by the same protocol with an additional sonication for 90 s at a power setting of 3 before placing the vial in a water bath at 85°C for 5 min prior to the sonication steps as in the standard protocol. These DSPC and DBPC lipid-only MBs (containing no PEG40S) were freshly prepared for each experiment due to their decreased stability.

For those experiments involving fluorescent labelling of MBs, a stock solution of the lipophilic dye 1,1'-dioctadecyl-3,3,3',3'-tetramethylindocarbocyanine perchlorate (DiI, Thermo Fisher Scientific Inc., USA) at a concentration of 2.5 mg/mL in dimethyl sulfoxide (DMSO, Sigma Aldrich, UK) was prepared. 7 μL of the stock solution were added to the lipid solution, and the protocols outlined previously were followed for MB production. In order to remove excess DiI from the formed MB suspension, the MB sample was centrifuged twice at 1000g for 10 min (400R Heraeus Labofuge, Thermo Fisher Scientific Inc., USA), and MBs were re-suspended in PBS after each centrifugation cycle. In order to assess the efficiency of MB shell labelling, fluorescent images were acquired at 63x magnification using a Zeiss LSM 780 confocal microscope (Carl Zeiss AG, Germany). For this purpose, a MB sample was placed between a 75 mm × 25 mm × 0.17 mm glass coverslip (Logitech Ltd., Scotland) and a 24 mm × 24 mm glass coverslip (VWR International, USA). A representative fluorescent image of DiI labelled MBs is shown in Fig. 1C, and the corresponding size distribution in Fig. 1D.

To prepare DSPC-PEG40S MBs washed by centrifugation, MBs were similarly loaded in a 10 ml syringe and centrifuged for 5 minutes at 200g. Following centrifugation,

the subnatent was discarded and the MBs resuspended in phosphate buffered saline (PBS) as described elsewhere [45].

For quantification of MB size and concentration, 10 μL of the MB suspension were transferred onto a Neubauer improved cell counting chamber (Hausser Scientific Company, USA) under a 24 mm × 24 mm glass coverslip (VWR International, USA). MBs were imaged at 40x magnification using a Leica DM500 microscope (Leica Microsystems GmbH, Germany) coupled with a CCD camera (MicroPublisher 3.3 RTV, QImaging, Canada). MB sizing and counting was performed using a purpose-written code in MATLAB® (The MathWorks Inc., USA) [46]. Fig. 1A shows a representative microscope image of the obtained DSPC-PEG40S MBs (the primary MB used in this study), with the corresponding size distribution of the same sample reported in Fig. 1B. MB mean diameter and concentration were equal to 1.59 ± 1.24 μm and 6.15×10^7 MBs/mL (for 945 MBs), 2.05 ± 1.59 μm and 6.14×10^7 MB/mL (for 8505 MBs), 1.69 ± 0.99 μm and 1.48×10^7 MBs/mL (for 174 MBs imaged at higher dilution and suspended in 5 mL PBS like the other formulations), 2.04 ± 1.59 μm and 5.93×10^7 MBs/mL (for 8737 MBs) for DSPC-PEG 9:1, DSPC-PEG 90:1, DSPC, and DBPC MBs respectively, and were measured by bright-field microscope images as described above. Washing DSPC-PEG40S 9:1 MBs resulted in a MB diameter of 2.18 ± 1.08 μm. For use in the experiments, washed MBs and DSPC MBs (a less stable formulation) were resuspended in 2 mL PBS (rather than 5 mL) to produce concentrations comparable to those of the other MB formulations.

2.4 Cell culture and sample preparation

A-549 cells, immortalized human alveolar adenocarcinomic cells, were grown in Dulbecco's Modified Eagle Medium (DMEM) with 10% fetal bovine serum (FBS) and 1% penicillin/streptomycin (P/S). CHO-K1 cells, immortalized Chinese hamster ovarian cells, were grown in Ham's F-12 medium with 10% FBS. Cells grown in T-75 flasks were passaged every three days at approximately 80% confluence. For experiments, approximately 1×10^6 cells were seeded in 80 mm diameter petri dishes containing a single 75 mm × 25 mm × 0.17 mm glass coverslip (Logitech Ltd., Scotland) in 10 mL growth medium. Coverslips were sterilized in 70% ethanol for 30 minutes followed by washing with phosphate buffered saline (PBS) and 30 minutes UV exposure prior to seeding. Cells were grown in a temperature- and CO_2-controlled incubator at 37°C and 5% CO_2. Cells were deemed ready for experiments at approximately 40% confluence at which point the cells on glass coverslips were carefully transported to the acoustofluidic device using sterile tweezers and washed twice with PBS. Sub-confluent cells were chosen for these experiments to improve the reliability of image analysis based on the quantification of membrane lipid order. For experiments involving measurement of membrane lipid order, cells were incubated with 400 nM C-Laurdan, a fluorescent probe used to sense lipid order in cells and artificial membranes, in PBS for 5 min prior to spectral imaging. It was determined that PBS was a suitable choice of medium for both imaging quality and cell viability given the short duration of the experiments.

For lipid transfer experiments, cells were labelled with CellMask Deep Red (Life Technologies, USA) diluted 1:100 in PBS and incubated for 10 min in the device. In

both experiments, the medium was gently replaced with fresh PBS prior to imaging, and cells were kept at 37°C using the temperature-controlled chamber of the confocal microscope (Zeiss LSM 780, Carl Zeiss AG, Germany) for the duration of the experiments. All cell culture materials were purchased from ThermoFisher Scientific (UK) unless stated otherwise.

2.5 Acoustofluidic device for microscopy-enabled ultrasound exposure

Acoustofluidic devices were designed for the generation of US fields within a confined microfluidic environment, containing either living cells or cell models (i.e., GUVs). A combination of acoustic, optical and biological criteria guided the design process, including: (i) generation of a spatially uniform acoustic pressure field at therapeutically relevant US frequencies, allowing for similar exposure conditions across the cell or GUV population; (ii) minimization of secondary effects of US exposure (i.e., acoustic streaming), to enable decoupling of the effects of US from those of US in combination with MBs; (iii) mimicking of the physical confinement typical of physiological microenvironments; (iv) coupling with low-working distance, oil immersion microscope objectives; (v) bio-compatibility; and (vi) ease of priming and reusability.

The design and fabrication of a multi-layered thin-reflector resonator [47] was chosen to satisfy the aforementioned requirements. A schematic of the device is shown in Fig. 2B. This multi-layered resonator comprises an US source, a carrier layer coupling the acoustic energy into the other layers of the device and isolating the transducer from the fluid layer, a fluid layer, and a thin-reflector layer to reduce acoustic reflections at the fluid-glass boundary compared with conventional designs in order to achieve a more uniform US field. Samples in the experiments were located in the fluid layer of the device either in suspension (GUVs or microbubbles) or adherent to the glass coverslip (cells).

A 13.0 mm × 30 mm × 1.0 mm piezoelectric element (PZ26, Meggit PLC, UK) was employed as US source and coupled to the carrier layer using a thin film of epoxy resin (RX771C/NC, Robnor Resins Ltd., UK) cured at 30°C for 24 h. The carrier layer was made of Macor (Ceramic Substrates & Components Ltd, UK), a machinable glass-ceramic material. The fluidic chamber architecture was milled into the carrier layer, using a computerized numerical control (CNC) milling machine (VM10, Hurco Companies, Inc., USA). The side walls of the chamber were formed by a custom moulded polydimethylsiloxane (PDMS) gasket (Sylgard® 184, Dow Corning Corporation, USA), which was obtained by mixing PDMS precursor and curing agent (10:1 w/w), followed by degassing and curing at 90°C for 1 h. The thickness of the carrier and fluid layers in the active region of the device (i.e., below the piezoelectric element) were equal to 1350 μm and 200 μm, respectively. The fluid layer was 12 mm wide, and had tapered sections nearby the inlet and outlet ports. The reflector layer was formed by a 75 mm × 25 mm × 0.17 mm glass coverslip (Logitech Ltd., Scotland). A milled Perspex® manifold permitted fluidic connectors to deliver fluid samples into the device (e.g. to introduce GUVs/microbubbles in suspension). Connection ports with 1/4''-28 flat-bottom thread were created through the manifold to join the inlet/outlet ports with 1.58 mm outer diameter and 0.5 mm

inner diameter tubing (Sigma Aldrich, UK). A metal frame with a central cut-out was employed to maintain stable contact between the layers.

A 1-dimensional (1-D) transfer impedance model implemented in MATLAB® (The MathWorks Inc., USA) was employed to design the thickness of each layer, in order to obtain the desired acoustic pressure field at the therapeutically relevant ~1 MHz US frequency. The modelled magnitude of acoustic pressure (normalised to the maximum value) at the first thickness resonance of the layered structure is reported in Fig. 2C. Notably, a relatively uniform acoustic pressure field in the direction of US propagation can be appreciated within the fluid layer of the device. The Reynolds stresses responsible for acoustic streaming patterns originate from gradients in acoustic energy density. Therefore designing for a uniform field distribution results in relatively low acoustic streaming velocities. Furthermore, given that the thickness of the reflector layer is significantly lower than the US wavelength (=0.033·λ), most of the incoming acoustic energy is reflected at the glass-air interface where a minimum in the acoustic pressure occurs (Fig. 2C). Thin-reflector resonators have also demonstrated reduced sensitivity to variations in the thickness of the constitutive layers, compared to other acoustofluidic configurations. Verification of the predicted resonance frequency (f ~ 0.97 MHz) was obtained experimentally.

2.6 Observing material transfer between cells and microbubbles by fluorescence microscopy

Material transfer between the MB shell and cell membrane was qualitatively assessed by confocal fluorescence microscopy. For this purpose, MBs were labelled with the lipophilic dye, DiI, whilst cells were labelled using CellMask Deep Red. Experiments were conducted using DSPC-PEG40S 9:1, DSPC, and DBPC MBs, with and without US exposure. Prior to adding MBs, the excitation laser power (<1.5%) and gain (750) were set such that minimal fluorescence signal from the DiI channel was observed. The medium was then replaced by the MB suspension. For experiments involving acoustic stimulation, US was applied immediately after adding the MBs. Following the incubation period, residual suspended MBs and shell fragments were washed away with PBS at a flow rate of 0.9 mL/min for 5 min. After washing, final fluorescence images were acquired. The experiment was repeated three times for each condition and additionally, images were taken with free DiI added to the medium with labelled cells. Colocalization of DiI and CellMask was confirmed by the Costes' method using the Coloc2 plugin in ImageJ (NIH, USA). Three-dimensional colocalization maps were obtained using MATLAB. Transfer of DiI to cell membranes was interpreted as a transfer of material from the microbubble shell to the cell membrane, but not necessarily as a transfer of phospholipids. The latter was confirmed upon complementing fluorescence intensity observations with spectral imaging data, as described in the following sections.

2.7 Exposure of GUVs to microbubbles and ultrasound

In order to quantify changes in the physical properties of DOPC GUVs under exposure to US and/or MBs, a range of different experimental conditions were investigated (see points *i-iv* below). Experiments were carried out at the ambient

temperature (~21ºC) and were repeated at least three times for each set of experimental conditions.

i. Control. The acoustofluidic device was placed on the microscope stage; GUVs were loaded into the device using a micropipette and optically imaged in the absence of external physical stimuli under static conditions (i.e., absence of fluid flow).

ii. Exposure to US. The acoustofluidic device loaded with GUVs was actuated by a radio frequency (RF) power amplifier (55 dB, Electronics & Innovation, Ltd., USA) driven by a sine-wave from a programmable signal generator (33220A, Agilent Technologies Inc., USA). An oscilloscope (HM2005, Hameg Instruments GmbH, Germany) was used to monitor the applied voltage and the operating frequency. GUVs were exposed to 60 sec continuous wave US at frequency and peak-to-peak rarefactional pressure of ~0.97 MHz and ~0.21 MPa, respectively. GUVs were imaged before and after exposure to US. The acoustic pressure in the layered acoustic resonator was measured using a calibrated fibre optic hydrophone (Precision Acoustics, UK) in a 0.5 mm diameter hole drilled through the reflector layer.

iii. Exposure to MBs. A mixture of GUVs and DSPC:PEG40S 9:1 MBs (at a final MB concentration of ~5×10^7 MBs/mL) was loaded into the device, and GUVs were imaged 60 sec after exposure to MBs. Microscope images of GUVs prior to MB exposure were also acquired.

iv. Exposure to US and MBs. The acoustofluidic device was loaded with a mixture of GUVs and DSPC:PEG40S 9:1 MBs (at a final MB concentration of ~5×10^7 MBs/mL). The device was actuated using the experimental conditions reported above in point *ii*. GUVs were imaged before and after exposure to US and MBs.

2.8 Exposure of cells to microbubbles and ultrasound

The same experimental conditions reported for GUVs were applied to living cells for quantifying membrane physical properties after exposure to MBs and/or US. Only minor modifications to the protocols were made, which are reported below. Experiments were carried out at 37ºC and were repeated at least three times for each experimental condition.

i. Control. The acoustofluidic device with a cell coated reflector was assembled and placed onto the microscope stage for cell imaging. Prior to imaging, 1-2 mL of PBS (kept at 37ºC) was slowly injected into the device using a 5 mL plastic syringe (BD, Becton, Dickinson and Company, USA) in order to remove any excess fluorophore from the extracellular medium. Images of the same cells were taken immediately after washing and after 60 sec, representative of the US exposure time used in other experimental conditions.

ii. Exposure to US. Cells were exposed to 60 sec US under the same acoustic conditions reported for GUVs. Sample washing and imaging protocols were the same as above (*i)*.

iii. Exposure to MBs. A suspension of MBs was prepared by mixing warm PBS (kept at 37ºC) with the stock MB suspension (kept at environmental temperature), to achieve a final MB concentration of ~5×10^7 MBs/mL. After cells washing (see step *i*), the MB suspension was injected into the device using a 5 mL plastic syringe (BD, Becton, Dickinson and Company, USA), and the same cells were imaged before and after exposure to MBs. Experiments were carried out using DSPC:PEG40S (9:1 and 90:1 molar ratio) and DSPC only MBs. Additionally, the effects of sonicated PEG40S and DSPC-PEG 9:1 MB washed by centrifugation on cell membrane lipid order were investigated.

iv. Exposure to US and MBs. After cell washing, the MB suspension was injected into the acoustofluidic device and cells were exposed to US as described previously. The same cells were imaged before and after exposure to MBs and US. Experiments were carried out using both DSPC:PEG40S 9:1 and DSPC MBs.

2.9 Measuring GUV membrane viscosity using fluorescence lifetime imaging microscopy

Variations in GUV membrane viscosity after exposure to US and/or MBs were quantified by applying fluorescence lifetime imaging microscopy (FLIM) to exploit the viscosity-sensitive photophysical properties of a molecular rotor (BODIPY-C_{12}), following a protocol previously reported [48]. Membrane labelling was carried out by adding BODIPY-C_{12} to the GUVs with an incubation time of 15 min. The maximum rotor concentration was set to 0.5 mol% (1:200 rotor:lipid) to prevent dye aggregation or a significant effect on the physical properties of the lipid bilayer [5, 49]. The acoustofluidic device was placed on the stage of a Leica SMD SP8 confocal microscope (Leica Microsystems Ltd., Germany) and lifetime images were obtained using an external TCSPC module (PicoHarp from PicoQuant, Germany) and an external photon counting spad detector (Pico Quant, Germany) until a minimum of 300 photons/pixel were acquired. FLIM data were analysed in SymPhoTime 64 software (PicoQuant, Germany), where a monoexponential model was fitted to each pixel lifetime decay. Thresholding was performed in order to remove background noise. Further data analysis (including statistical analysis and data plotting) was carried out using OriginPro 9.1 (OriginLab Corporation, USA).

2.10 Measuring GUV lipid diffusion using fluorescence correlation spectroscopy

Changes in membrane lipid diffusion dynamics after exposure to US and/or MBs were quantified using the fluorescence correlation spectroscopy (FCS) unit of a Zeiss LSM 780 confocal microscope (Carl Zeiss AG, Germany). The lipid analogue cholesterol-PEG-KK114 was employed as a fluorescent probe in these experiments, and added to the GUV suspension at a concentration of 0.1 mol% with an incubation time of 15 min. FCS was carried out following a protocol previously reported [50]. FCS uses the confocal microscope to detect trace amounts of fluorophore passing through a tiny (i.e., sub-femtoliter) detection volume, which is created by focusing a laser to a diffraction-limited spot using a high-numerical aperture objective. The detected fluctuating fluorescence intensity signal $F(t)$ is autocorrelated, and the

obtained autocorrelation function relates to the probability that a signal detected at different time instants belongs to the same molecular event. The decay time of the autocorrelation function relates to the residence time of the fluorophore within the detection volume.

In this study, the focal spot was placed at the bottom of the GUV (but could also be placed at the top with the results remaining unchanged), with the optical settings kept identical for acquisitions taken either before or after exposure to US and/or MBs. The average transit time of the fluorophores through the focal spot was calculated by fitting the autocorrelation function $G(\tau)$ to a two-dimensional one-component diffusion model [51]:

$$G(\tau) = \frac{1}{N}\left(1+\frac{\tau}{\tau_D}\right)^{-1} \qquad \text{Eq.1}$$

where N is the average number of fluorescent particles in the detection volume, τ is the correlation time, and τ_D the average transit time. τ_D was determined as an indicator of lipid diffusion dynamics, at the different experimental conditions reported previously. Higher τ_D corresponded to a slower diffusion process, and was therefore associated with increased membrane viscosity and lipid order. Autocorrelation functions were processed using the microscope built-in software ZEN (Carl Zeiss AG, Germany), and further data analysis (including statistical analysis and data plotting) was carried out using OriginPro 9.1 (OriginLab Corporation, USA).

2.11 Measuring GUV and cell plasma membrane lipid order using spectral imaging

Changes in the lateral order of the lipids (revealing how densely the lipids are packed) due to exposure to US and/or MBs were quantified using C-Laurdan, an environmentally-sensitive fluorescent probe with the same spectral characteristics as Laurdan, but with greater photostability. Cells and GUVs were incubated with C-Laurdan (400 nM) for 5 and 15 min, respectively. The emission spectrum of Laurdan shifts as a function of the dipolar water relaxation, and thus the level of hydration within its surrounding microenvironment, which in turn is indicative of relative lipid packing [52]. Spectral imaging was carried out on a Zeiss LSM 780 confocal microscope equipped with a 32-channel GaAsP detector array, following a method previously reported [53]. C-Laurdan was excited at 405 nm and the lambda detection range was set between 415 nm and 691 nm. Generalized polarization (GP, ranging from -1 to 1) was employed as a relative measure of lipid packing, and was calculated as follows [54]:

$$GP = \frac{I_{440} - I_{490}}{I_{440} + I_{490}} \qquad \text{Eq. 2}$$

Where I_{440} and I_{490} correspond to the fluorescence intensity at 440 nm and 490 nm emission wavelengths, respectively. Notably, 440 nm corresponds to a blue emission in the wavelength spectrum and is associated with low fluidity and polarity, resulting in GP = +1 when only this wavelength is emitted. This indicates higher lipid order and means that lipids are in the gel-phase (ordered). Conversely, 490 nm corresponds to

a red emission and is associated with high fluidity and polarity, resulting in GP = -1. This indicates lower lipid order and means that the lipids are in the liquid-crystalline phase (disordered, or less ordered).

Therefore, a high GP value describes a low amount of water in the vicinity of the C-Laurdan probe, and consequently, a high degree of lipid order. GP of artificial membranes was quantified using a custom plug-in compatible with Image J and data analysed using OriginPro 9.1 (OriginLab Corporation, USA), whilst a custom image processing routine was developed in MATLAB for performing membrane segmentation and GP calculation in experiments utilising cells. Briefly, images of cells at 440 nm and 490 nm before and after treatment were thresholded automatically by the Otsu's histogram method (Fig. 3A-B). Objects of interest were then segmented and cropped using connected-component labelling of the binary thresholding mask followed by the watershed transform method. From these images, a pseudo-coloured GP map was generated for each cell (Fig. 3C) and cell membranes were segmented by taking a five pixel border around each cell (Fig. 3D). Successful segmentation was manually verified for each image in the analysis. Average GP values at the different exposure conditions investigated were determined for experiments involving GUVs suspended in the fluid channel, while a ΔGP value could be determined for the adherent cells, as the same cell could be imaged before and after exposure.

2.12 Statistical analysis of the results

For statistical analysis of experiments with GUV model membranes or CHO-K1 cells, one-way analysis of variance (ANOVA) was employed. For statistical analysis of experiments with A-549 cells, a multiway ANOVA was employed with PEG40S concentration, lipid chain length, and ultrasound exposure as factors. All ANOVAs were followed with multiple comparisons using Tukey-Kramer tests (significant for $p < 0.01$).

3. Results

3.1 Observations of lipid transfer from microbubbles to cell membranes

Material transfer from DSPC-PEG40S, DSPC, and DBPC MBs to A-549 cells with and without US exposure was investigated using confocal fluorescence microscopy. A green fluorescent membrane probe (DiI) was employed to stain the MBs and to indicate material transfer from the MBs, and a red fluorescent membrane stain (CellMask) was employed to mark the cellular plasma membrane (Fig. 4). The fluorescence images highlight that following US exposure, DiI was transferred to the cellular membranes for all three MB formulations, with a diffuse pattern for DSPC-PEG40S (likely indicating integration within the membrane) (Fig. 4D) and a punctate pattern for DSPC and DBPC (potentially indicating formation and transfer via lipid vesicles or aggregates) (Fig. 4E and 4F). Without US exposure, significant DiI transfer was observed for DSPC MBs (in form of vesicles), but not for DSPC-PEG40S and DBPC MBs. Three-dimensional Costes' method colocalization of DiI and CellMask from a

confocal z-stack, demonstrates that DiI was extensively colocalized with cell membranes for the case of DSPC-PEG40S MB and US exposure (Fig. 4G). From these observations, integration of MB material into cell membranes was qualitatively assessed but not specifically quantified by DiI colocalization. Quantification of this process was performed by complementing qualitative observations with spectral imaging using C-Laurdan, as described in the following sections.

3.2 Changes in membrane properties in model membranes exposed to US and MB

We next investigated how the lipid transfer from the MBs to the cellular membranes induced changes in the membrane properties. For this, we first investigated the following biophysical properties: membrane viscosity, lipid order, and lipid mobility in giant unilamellar vesicles (GUVs) made of DOPC following exposure to US and/or DSPC-PEG40S MBs (Fig. 5). These properties all reveal how densely the lipids are packed within the membrane.

Fluorescence lifetime of the molecular rotor BODIPY-C_{12} was employed as an indicator of membrane viscosity and was measured using fluorescence lifetime imaging microscopy (FLIM) [48] (Fig. 5A). In molecular rotors the non-radiative deactivation rate, and therefore the fluorescence lifetime, changes depending on the viscosity of the immediate membrane microenvironment. The presence of DSPC-PEG40S MBs significantly increased rotor lifetime in DOPC GUVs, signifying increased membrane viscosity with and without US exposure (lifetime was equal to 2.17 ± 0.10 ns and 1.96 ± 0.25 ns with and without US, respectively, compared to 1.61 ± 0.10 ns for the sham control; $p < 0.01$), while no increase in fluorescence lifetime was observed following exposure to US only (i.e. without MBs; 1.62 ± 0.07 ns).

These observations were corroborated by measurements of C-Laurdan fluorescence as a reporter of lipid lateral order within the plane of a membrane. The fluorescence spectrum of C-Laurdan shifts to the blue for more ordered membrane environments. Comparing signal intensities observed in the blue- and red-shifted regime of C-Laurdan emission spectrum thus allows for the determination of the generalized polarization (GP), which takes larger values for more ordered membrane environments (see Materials and Methods section) (Fig. 5B). Results show a statistically significant increase in lipid order in the presence of DSPC-PEG40S MBs, with and without US (GP = -0.37 ± 0.09 and -0.44 ± 0.07 with and without US, respectively, while GP = -0.52 ± 0.05 without treatment and -0.47 ± 0.04 after exposure to US only, $p < 0.01$).

With both of these techniques, it was found that US enhanced the measured effect from exposure to MBs. This result was further supported by comparing the average transit time through the microscope observation spot of a GUV membrane-embedded fluorescent analogue (cholesterol-PEG-KK114) as measured by fluorescent correlation spectroscopy (FCS) (Fig. 5C). This transit time is a measure of the mobility of lipids within the GUV membrane, and thus another indicator of membrane viscosity. DSPC-PEG40S MBs caused a statistically significant increase in

lipid diffusion time (i.e., from control value of 1.55 ± 0.07 ms to 1.82 ± 0.22 ms) when exposed to US ($p < 0.01$). In the absence of US, MBs caused only a slight increase in mean lipid diffusion time in GUVs (i.e., from 1.55 ± 0.07 ms to 1.60 ± 0.08 ms), however this was not statistically significant ($p > 0.01$).

3.3 Changes in lipid order in cell membranes exposed to US and MB

In the next step, we investigated changes in lipid order (or packing) in cellular membranes. C-Laurdan generalized polarization (GP) was evaluated in the plasma membrane of A-549 cells after exposure to MBs of different composition with and without US. To compensate cell-to-cell heterogeneity, we measured general polarization values on individual cells before (GP_{before}) and after (GP_{after}) exposure to MBs and/or US and calculated the difference $\Delta GP = GP_{after} - GP_{before}$, which was used as a metric for the effect of MBs and/or US on membrane lipid order. Negative or positive values of ΔGP indicate a decrease or an increase in membrane lipid order, respectively. Due to the variation in GP values of cell membranes before treatment, there is corresponding variation in ΔGP values. This variation is to be expected given the highly nonlinear responses of biological systems to factors affecting lipid order. Nonetheless, by quantifying the change in lipid order on a single cell basis with the ΔGP parameter, significant insights into the response of cell membranes to various treatments could be obtained. Depending on the composition of the MBs, we observed both increases as well as decreases in lipid order compared to controls (Fig. 7). Representative membrane GP maps can be seen in Fig. 6 for exposure of cells to the control (in the absence of US and MBs), DSPC-PEG40S MBs (decreased GP), and DSPC MBs (increased GP) with and without US exposure respectively.

3.3.1 Dependence on PEG40S concentration

To evaluate the effect of the molar ratio of DSPC to PEG40S in the MB formulation on lipid order in A-549 cells, the cells were exposed to MB of molar ratio 9:1, 90:1 and 1:0 (DSPC only MBs) with and without US exposure respectively, and to sonicated PEG40S (no MBs). The presence of PEG40S in all cases significantly decreased lipid order ($\Delta GP = -0.035 \pm 0.050$, $\Delta GP = -0.035 \pm 0.075$, and $\Delta GP = -0.157 \pm 0.076$ for cells exposed to MB with a 9:1 or 90:1 molar ratio or to sonicated PEG40S respectively, $p < 0.01$) (Fig. 7). Conversely, DSPC MB without PEG40S (1:0 molar ratio) were found to significantly increase lipid order in A-549 cell membranes ($\Delta GP = 0.050 \pm 0.049$ and $\Delta GP = 0.044 \pm 0.049$ with and without US exposure respectively, $p < 0.01$) (Fig. 7).

Since lowering PEG40S concentration by an order of magnitude had no significant effect on the induced membrane disordering in A-549 cells, the effect of washing DSPC-PEG40S 9:1 MB by centrifugation (in an attempt to reduce levels of PEG40S in solution) was investigated. It was found that in contrast to the unwashed case, washed MB increased lipid order in A-549 cell membranes ($\Delta GP = 0.034 \pm 0.027$ and $\Delta GP = 0.047 \pm 0.039$ for exposure to washed MB with and without US respectively, in contrast with $\Delta GP = -0.042 \pm 0.057$ and $\Delta GP = -0.035 \pm 0.050$ for the unwashed case, $p < 0.01$) (Fig. 7).

3.3.2 Influence of lipid chain length

Membrane lipid order depends on, among other factors, the chain length of lipids in a membrane. Therefore we investigated the effect of lipid chain length in the MB formulation on the resultant changes in lipid order of A-549 cell membranes. Since, as above, PEG40S had a strong effect on membrane lipid order even at low concentrations, the use of PEG40S was avoided in these experiments. It was found that lipid chain lengths lower than that of DSPC (18:0 PC) would not readily form stable microbubbles in the absence of PEG40S. Thus, only MBs composed of DSPC (18:0 PC) and the higher lipid chain length DBPC (22:0 PC) were investigated, with and without US exposure. It was found that while exposure to DSPC MBs significantly increased lipid order, exposure to DBPC MBs did not have a significant effect ($\Delta GP = -0.023 \pm 0.050$ and $\Delta GP = -0.005 \pm 0.044$ for DBPC MBs with and without US exposure respectively, $p > 0.01$) (Fig. 8). Yet, as highlighted before, we could in both cases observe some material transfer from the MBs to the cell membrane (Fig. 1), which was more pronounced with US exposure. The role of lipid chain length in material transfer from MBs to cell membranes will be discussed further in Section 4.3.

3.3.3 Observations in different cell lines

To determine whether the aforementioned effects are specific to A-549 cells only, we repeated measurements of changes in lipid order after lipid transfer from MBs in ovarian hamster (CHO-K1) cells. Again, a significant decrease in cell membrane lipid order was found following exposure to DSPC-PEG40S 9:1 MBs with and without US ($\Delta GP = -0.035 \pm 0.048$ and $\Delta GP = -0.010 \pm 0.050$ respectively, $p < 0.01$) (Fig. 9), which is in agreement with observations for the same experimental conditions in A-549 cells.

4. Discussion & Conclusions

Using different fluorescence microscopy tools, we have characterized changes in lipid membrane order, i.e. how tightly lipids are packed in membranes after transfer of material from microbubbles (MBs) with or without the presence of ultrasound (US). Together our findings demonstrate that even in the absence of US exposure, the MB solution can significantly alter membrane properties in a formulation-dependent manner

4.1 Evidence for material transfer

DiI, a lipophilic dye with molecular dynamics comparable to those of lipids was used as a means of visualizing MB-membrane interaction. Following exposure of cells to DiI-loaded DSPC MBs, co-localization of DiI with cell membranes was observed (Fig. 4). Direct transfer of therapeutics from the MB shell to cellular membranes via MB-cell fusion, MB destruction, and/or lipid shedding, is a candidate mechanism for the enhancement of US-mediated drug delivery produced by phospholipid-coated MBs [25, 28, 30]. Inter-vesicular transfer of lipids between membrane bilayers in model

systems is a well-known process, and has previously been demonstrated [55]. Moreover, a recent study by De Cock and co-authors reported evidence for deposition of MB constituents onto the cell membrane that were subsequently internalized by cells [56]. Our current study complements these observations of material transfer from MB coatings to cell membranes by the quantification of changes in cell membrane biophysical properties, as discussed in the following sections.

4.2 Transfer to model membranes – biophysical properties

We used model membranes (GUVs) and measures of membrane viscosity, lipid order, and lipid mobility to test the feasibility of our approach to determine lipid packing in membranes following exposure to MBs (with and without US) (Fig. 5).

DOPC GUVs exposed to DSPC-PEG40S MBs exhibited increased lipid order, a change that was most significant when observed by changes in membrane viscosity (Fig. 5A). This increase in lipid order could be the result of a transfer of highly saturated DSPC lipids to GUV membranes. As a highly disordered system, the lipid order of DOPC GUVs would be much more sensitive to such a change in composition than more ordered membranes (DOPC GUVs were chosen for precisely this reason). It is also conceivable, however, that in the disordered DOPC GUVs, PEG40S could have a lipid ordering effect rather than the disordering effect seen in cell membranes. In agreement with this supposition, Lehtonen and Kinnunen reported decreased membrane fluidity in DOPC liposomes exposed to PEG [57]. PEG, a highly hygroscopic polymer, could increase lipid order in disordered systems by inducing osmotic stress at either the membrane-fluid interface, leading to dehydration of phospholipid headgroups, or across the membrane, leading to osmotic shrinkage [22].

Although the presence of PEG40S adds complexity to interpreting the effects of DSPC-PEG40S MBs on DOPC GUVs, these results nonetheless suggest lipid transfer in addition to an ordering effect from the PEG40S. Since PEG40S appears to be excluded from DSPC-PEG40S MB shells upon formation [58], the concentration of PEG40S that the sample is exposed to following US exposure is not expected to increase substantially. Thus, US-mediated liberation of PEG40S from MB shells is not expected to influence lipid order [57]. Formation of reactive oxygen species (ROS) can also increase lipid order [59]; however, singlet oxygen formation from comparable US exposures of phospholipid MBs has been shown to be minimal and is not expected to play a critical role here [44]. Thus, the increase in the lipid order of DOPC GUVs exposed to DSPC-PEG40S MBs and US provides additional support for our lipid transfer hypothesis while demonstrating the feasibility of our experimental approach.

4.3 Lipid transfer to live cell membranes – changes in lipid order

In agreement with the direct visualization of material transfer from MBs to cells, we were able to quantify significant changes in lipid order in cell plasma membranes following exposure to MBs. As expected from the GUV measurements, the lipid order of cell membranes significantly increased in the presence of DSPC MBs, suggesting integration of saturated DSPC lipids (Fig. 7). This finding is particularly important because lipid order has been shown to influence cell signaling, membrane protein folding, junctional integrity, and intracellular permeability [60]. Specifically, regarding the relevance and magnitude of the observed effects, comparable changes in GP have been associated with very large changes in the cholesterol content (e.g. by ~10% in DPPC vesicles [61]), the pH (e.g. from 4.1 to 7.4 in DPPS:DPPC vesicles [62]), the temperature (e.g. in DMPC GUVs at 37°C vs 34°C [52]), or the phospholipid composition (e.g. DLPC vs DPPC, at 20°C [62]) in model membranes.

Exposure of the cell membranes to DBPC MBs (22:0 PC compared to 18:0 PC for DSPC, i.e. longer lipid chains), however, did not induce a significant change in lipid order in cell membranes. It also resulted in punctate DiI fluorescence following US, and negligible fluorescence without US exposure. This suggests that it is energetically favorable for long-chained DBPC lipids to stay in the MB shell or form liposomes, rather than integrating into cell membranes. This may be explained by the higher melting temperature of DBPC (73.6 ± 2.1 °C) compared to DSPC (54.5 ± 1.5 °C) [63], and the exponential relationship between lipid chain length and MB shell gas permeation resistance [64]. From a drug delivery perspective, these results suggest that DSPC is better suited to transferring material to cell membranes than lipids with longer chains.

4.4 Lipid transfer to live cell membranes – influence of PEG40S

The presence of PEG40S in the MBs significantly decreased lipid order in cellular membranes and even induced negligible transfer of DiI without US exposure (Fig. 4 and Fig. 7). It was subsequently found that cells exposed to PEG40S alone (i.e. without MBs) also exhibited significantly lower lipid order (Fig. 7), indicating that the presence of PEG40S in the MB coating leads to a significant disordering of the cell membranes. Previous studies on both lipid and cell-derived plasma membrane models have shown that there is a non-linear relationship between lipid order and the concentration of PEG in the surrounding solution and that this is also dependent upon temperature, pH, chain length, molecular weight, concentration, and lipid composition [57, 60, 65]. In cells, the mechanisms underlying the PEG-induced decrease in lipid order may include membrane phospholipid hydration, conformational changes in membrane proteins, incorporation in the cell membrane, or binding with membrane carbohydrates and proteins. At the same pH used in our experiments, for instance, it has been shown that PEG-induced conformational changes in proteins are increased, and the role of cholesterol in restoring lipid order is diminished [65]. Similarly, in agreement with our results, membrane fluidity (inversely proportional to lipid order) has been shown to increase in erythrocytes and erythrocyte ghosts exposed to PEG at the same pH and temperature [65, 66].

The membrane disordering effect of PEG40S is further supported following exposure of cells to DSPC-PEG40S MBs washed by centrifugation (Fig. 7). We observed that washing these MBs, effectively removing free PEG40S, led again to an increase in lipid order, explained by the transfer of highly saturated DSPC lipids to cell membranes. The latter is supported by the fact that the increase in membrane order after exposure to the washed DSPC-PEG40S MBs was similar to that observed for MBs formed from DSPC without PEG40S. Since PEG40S is widely recognized as beneficial to the formation of MBs, it is interesting to note that by the washing technique employed here, the benefits of PEG40S on MB formation may be realized without the disordering effect of PEG40S on cell membranes [48, 60].

4.5 Relevance to US-mediated drug delivery

Upon US exposure, MBs can induce mechanical, chemical and thermal effects that can influence the cell membrane and would be expected to affect lipid order. For instance, shear stress induced by US and MBs might be expected to decrease lipid order [67-69], while ROS generation may increase it [59]. Degradation of the actin cytoskeleton, opening of ion channels, formation of non-specific pores, blebbing, and rapid hyperpolarization of the cell membrane are all examples of reported US-mediated bio-effects that are indicative of a change in lipid order [12, 24, 27, 32, 70-72].

Interestingly, despite our observations of clear mechanical effects of US and MBs in our setup (i.e., cavitation microstreaming, microbubble destruction, and changes in cell conformation), US was not a statistically significant factor in changing lipid order in its own right across all cases studied. However, it is likely to play a role in facilitating microbubble cell contact. Moreover, since we measure changes in lipid order occurring within minutes of exposure, changes occurring on shorter timescales may not have been detected. Measuring the dynamic response of cell membranes exposed to MBs and US will be the subject of subsequent investigations and will require further developments to the current experimental system. In addition, the variation (i.e., standard deviation of the experimental data) in the response of cell membranes to MBs was reduced with US exposure in both cell lines investigated, suggesting a more subtle role for US in the observed effects on lipid order (Fig. 9).

Nonetheless, the effects on membrane lipid order produced by PEG40S and DSPC may have significant implications for US-mediated drug delivery. For instance, the most extensive transfer of DiI from DiI-loaded MBs was observed for MBs containing DSPC and PEG40S in a 9:1 molar ratio (Fig. 4), a formulation which also induced significant membrane disordering (Fig. 7). This could be a desirable effect for US-mediated drug delivery whereby PEG40S increases membrane fluidity, facilitating the incorporation of microbubble shell components (i.e., bioactive molecules) into cell membranes. Although PEG is not required for successful US-mediated drug delivery with MBs, e.g. with polymer or protein shelled MBs [73, 74], successful drug delivery with PEG-containing MBs has indeed been demonstrated extensively [9,11,14,64]. Considering that all current commercial phospholipid-coated MB

formulations contain PEG derivatives [75, 76], this effect could play a significant role in many US-mediated drug delivery studies.

For phospholipid-shelled microbubbles, which are commonly formed in the presence of an emulsifier such as PEG40S, our results present a previously unknown MB formulation-dependent bio-effect that could have implications for US-mediated drug delivery. Furthermore, our work strongly supports the transfer of MB shell components to cell membranes, a phenomenon hypothesized to play a role in US-mediated drug delivery. Lastly, because the effects observed occurred without US exposure, we hypothesize that changing cell membrane lipid order with a certain MB formulation, hence changing the mechanical properties of the cell membrane, could induce a priming effect in cells for other US-mediated bio-effects. This final aspect will be the subject of future research.

Acknowledgments

We would like to extend our gratitude to Dr. Shamit Shrivastava for most helpful discussions, James Fisk and David Salisbury for the fabrication of the acoustofluidic devices, Dr. Joshua Owen for providing MB formulation protocols, and to Falk Schneider for assistance with GUV preparation. This work was supported financially by the Engineering and Physical Sciences Research Council (EPSRC EP/I021795/1). JBdlS acknowledges support from a Marie Curie Career Integration Grant. CE, ES, JBdlS thank financial support by the Wellcome Trust (grant ref 104924/14/Z/14), the Medical Research Council (grant number MC_UU_12010/unit programmes G0902418 and MC_UU_12025), MRC/BBSRC/ESPRC (grant number MR/K01577X/1), and institutional funding from the University of Oxford, and the Wolfson Imaging Centre Oxford (Christoffer Lagerholm, Esther Garcia and Dominic Waithe) for providing microscope facility support and Sumita Ganguly for general lab support.

References

[1] Lindner JR. Microbubbles in medical imaging: current applications and future directions. Nature Reviews Drug Discovery. 2004;3:527-33.

[2] Unger EC, Porter T, Culp W, Labell R, Matsunaga T, Zutshi R. Therapeutic applications of lipid-coated microbubbles. Advanced drug delivery reviews. 2004;56:1291-314.

[3] Abou-Saleh RH, Swain M, Evans SD, Thomson NH. Poly (ethylene glycol) lipid-shelled microbubbles: abundance, stability, and mechanical properties. Langmuir. 2014;30:5557-63.

[4] van Rooij T, Daeichin V, Skachkov I, de Jong N, Kooiman K. Targeted ultrasound contrast agents for ultrasound molecular imaging and therapy. International Journal of Hyperthermia. 2015.

[5] Hosny NA, Mohamedi G, Rademeyer P, Owen J, Wu Y, Tang M-X, et al. Mapping microbubble viscosity using fluorescence lifetime imaging of molecular rotors. Proceedings of the National Academy of Sciences. 2013;110:9225-30.

[6] Lentacker I, De Smedt SC, Sanders NN. Drug loaded microbubble design for ultrasound triggered delivery. Soft matter. 2009;5:2161-70.

[7] Klibanov AL. Ligand-carrying gas-filled microbubbles: ultrasound contrast agents for targeted molecular imaging. Bioconjugate chemistry. 2005;16:9-17.
[8] Frenkel PA, Chen SY, Thai T, Shohet RV, Grayburn PA. DNA-loaded albumin microbubbles enhance ultrasound-mediated transfection in vitro. Ultrasound Med Biol. 2002;28:817-22.
[9] Lentacker I, De Geest BG, Vandenbroucke RE, Peeters L, Demeester J, De Smedt SC, et al. Ultrasound-responsive polymer-coated microbubbles that bind and protect DNA. Langmuir. 2006;22:7273-8.
[10] Chen SY, Ding JH, Bekeredjian R, Yang BZ, Shohet RV, Johnston SA, et al. Efficient gene delivery to pancreatic islets with ultrasonic microbubble destruction technology. P Natl Acad Sci USA. 2006;103:8469-74.
[11] Hu Y, Wan JM, Alfred C. Membrane perforation and recovery dynamics in microbubble-mediated sonoporation. Ultrasound in medicine & biology. 2013;39:2393-405.
[12] Fan Z, Liu H, Mayer M, Deng CX. Spatiotemporally controlled single cell sonoporation. Proceedings of the National Academy of Sciences. 2012;109:16486-91.
[13] Kudo N, Okada K, Yamamoto K. Sonoporation by single-shot pulsed ultrasound with microbubbles adjacent to cells. Biophysical journal. 2009;96:4866-76.
[14] Honda H, Kondo T, Zhao QL, Feril LB, Kitagawa H. Role of intracellular calcium ions and reactive oxygen species in apoptosis induced by ultrasound. Ultrasound Med Biol. 2004;30:683-92.
[15] van Rooij T, Skachkov I, Beekers I, Lattwein KR, Voorneveld JD, Kokhuis TJ, et al. Viability of endothelial cells after ultrasound-mediated sonoporation: Influence of targeting, oscillation, and displacement of microbubbles. Journal of controlled release : official journal of the Controlled Release Society. 2016;238:197-211.
[16] Zhong WJ, Sit WH, Wan JMF, Yu ACH. Sonoporation Induces Apoptosis and Cell Cycle Arrest in Human Promyelocytic Leukemia Cells. Ultrasound Med Biol. 2011;37:2149-59.
[17] Van Wamel A, Kooiman K, Harteveld M, Emmer M, Folkert J, Versluis M, et al. Vibrating microbubbles poking individual cells: drug transfer into cells via sonoporation. Journal of Controlled Release. 2006;112:149-55.
[18] van Wamel A, Bouakaz A, Versluis M, de Jong N. Micromanipulation of endothelial cells: ultrasound-microbubble-cell interaction. Ultrasound in medicine & biology. 2004;30:1255-8.
[19] De Cock I, Zagato E, Braeckmans K, Luan Y, de Jong N, De Smedt SC, et al. Ultrasound and microbubble mediated drug delivery: Acoustic pressure as determinant for uptake via membrane pores or endocytosis. Journal of Controlled Release. 2015;197:20-8.
[20] Delalande A, Leduc C, Midoux P, Postema M, Pichon C. Efficient Gene Delivery by Sonoporation Is Associated with Microbubble Entry into Cells and the Clathrin-Dependent Endocytosis Pathway. Ultrasound in medicine & biology. 2015.
[21] Wu J, Ross JP, Chiu J-F. Reparable sonoporation generated by microstreaming. The Journal of the Acoustical Society of America. 2002;111:1460-4.
[22] Zhou Y, Yang K, Cui J, Ye J, Deng C. Controlled permeation of cell membrane by single bubble acoustic cavitation. Journal of Controlled Release. 2012;157:103-11.

[23] Marmottant P, Hilgenfeldt S. Controlled vesicle deformation and lysis by single oscillating bubbles. Nature. 2003;423:153-6.
[24] Pommella A, Brooks NJ, Seddon JM, Garbin V. Selective flow-induced vesicle rupture to sort by membrane mechanical properties. Scientific reports. 2015;5.
[25] Meijering BD, Juffermans LJ, van Wamel A, Henning RH, Zuhorn IS, Emmer M, et al. Ultrasound and microbubble-targeted delivery of macromolecules is regulated by induction of endocytosis and pore formation. Circulation research. 2009;104:679-87.
[26] Kooiman K, van der Steen AF, de Jong N. Role of intracellular calcium and reactive oxygen species in microbubble-mediated alterations of endothelial layer permeability. Ultrasonics, Ferroelectrics, and Frequency Control, IEEE Transactions on. 2013;60:1811-5.
[27] Juffermans LJ, van Dijk A, Jongenelen CA, Drukarch B, Reijerkerk A, de Vries HE, et al. Ultrasound and microbubble-induced intra-and intercellular bioeffects in primary endothelial cells. Ultrasound in medicine & biology. 2009;35:1917-27.
[28] Dijkmans P, Juffermans L, Musters R, van Wamel A, Ten Cate F, van Gilst W, et al. Microbubbles and ultrasound: from diagnosis to therapy. European Heart Journal-Cardiovascular Imaging. 2004;5:245-6.
[29] Kheirolomoom A, Dayton PA, Lum AF, Little E, Paoli EE, Zheng H, et al. Acoustically-active microbubbles conjugated to liposomes: characterization of a proposed drug delivery vehicle. Journal of Controlled Release. 2007;118:275-84.
[30] Der Loughian C, Seya PM, Pirat C, Inserra C, Béra J-C, Rieu J-P. Jumping acoustic bubbles on lipid bilayers. Soft matter. 2015;11:3460-9.
[31] Lentacker I, De Cock I, Deckers R, De Smedt S, Moonen C. Understanding ultrasound induced sonoporation: definitions and underlying mechanisms. Advanced drug delivery reviews. 2014;72:49-64.
[32] Leow RS, Wan JM, Alfred C. Membrane blebbing as a recovery manoeuvre in site-specific sonoporation mediated by targeted microbubbles. Journal of The Royal Society Interface. 2015;12:20150029.
[33] Owen DM, Rentero C, Magenau A, Abu-Siniyeh A, Gaus K. Quantitative imaging of membrane lipid order in cells and organisms. Nature protocols. 2012;7:24-35.
[34] McIntosh TJ, Simon SA. Roles of bilayer material properties in function and distribution of membrane proteins. Annu Rev Biophys Biomol Struct. 2006;35:177-98.
[35] Schäfer LV, de Jong DH, Holt A, Rzepiela AJ, de Vries AH, Poolman B, et al. Lipid packing drives the segregation of transmembrane helices into disordered lipid domains in model membranes. Proceedings of the National Academy of Sciences. 2011;108:1343-8.
[36] Olbrich K, Rawicz W, Needham D, Evans E. Water permeability and mechanical strength of polyunsaturated lipid bilayers. Biophysical journal. 2000;79:321-7.
[37] Xia WJ, Onyuksel H. Mechanistic studies on surfactant-induced membrane permeability enhancement. Pharmaceutical research. 2000;17:612-8.
[38] Fenz SF, Sengupta K. Giant vesicles as cell models. Integrative Biology. 2012;4:982-95.
[39] Amaro M, Sachl R, Jurkiewicz P, Coutinho A, Prieto M, Hof M. Time-Resolved Fluorescence in Lipid Bilayers: Selected Applications and Advantages over Steady State. Biophysical Journal. 2014;107:2751-60.

[40] Angelova MI, Dimitrov DS. Liposome electroformation. Faraday discussions of the Chemical Society. 1986;81:303-11.
[41] Sezgin E, Levental I, Grzybek M, Schwarzmann G, Mueller V, Honigmann A, et al. Partitioning, diffusion, and ligand binding of raft lipid analogs in model and cellular plasma membranes. Biochimica et Biophysica Acta (BBA)-Biomembranes. 2012;1818:1777-84.
[42] Helfield BL, Cherin E, Foster FS, Goertz DE. Investigating the subharmonic response of individual phospholipid encapsulated microbubbles at high frequencies: A comparative study of five agents. Ultrasound in medicine & biology. 2012;38:846-63.
[43] Gong Y, Cabodi M, Porter TM. Acoustic investigation of pressure-dependent resonance and shell elasticity of lipid-coated monodisperse microbubbles. Applied Physics Letters. 2014;104:074103.
[44] McEwan C, Owen J, Stride E, Fowley C, Nesbitt H, Cochrane D, et al. Oxygen carrying microbubbles for enhanced sonodynamic therapy of hypoxic tumours. Journal of Controlled Release. 2015;203:51-6.
[45] Feshitan JA, Chen CC, Kwan JJ, Borden MA. Microbubble size isolation by differential centrifugation. Journal of colloid and interface science. 2009;329:316-24.
[46] Sennoga CA, Mahue V, Loughran J, Casey J, Seddon JM, Tang M, et al. On sizing and counting of microbubbles using optical microscopy. Ultrasound in medicine & biology. 2010;36:2093-6.
[47] Carugo D, Octon T, Messaoudi W, Fisher AL, Carboni M, Harris NR, et al. A thin-reflector microfluidic resonator for continuous-flow concentration of microorganisms: a new approach to water quality analysis using acoustofluidics. Lab on a Chip. 2014;14:3830-42.
[48] Wu Y, Štefl M, Olzyńska A, Hof M, Yahioglu G, Yip P, et al. Molecular rheometry: direct determination of viscosity in L o and L d lipid phases via fluorescence lifetime imaging. Physical Chemistry Chemical Physics. 2013;15:14986-93.
[49] López-Duarte I, Vu TT, Izquierdo MA, Bull JA, Kuimova MK. A molecular rotor for measuring viscosity in plasma membranes of live cells. Chemical Communications. 2014;50:5282-4.
[50] Kahya N, Scherfeld D, Schwille P. Differential lipid packing abilities and dynamics in giant unilamellar vesicles composed of short-chain saturated glycerol-phospholipids, sphingomyelin and cholesterol. Chemistry and physics of lipids. 2005;135:169-80.
[51] Czogalla A, Petrov EP, Kauert DJ, Uzunova V, Zhang Y, Seidel R, et al. Switchable domain partitioning and diffusion of DNA origami rods on membranes. Faraday discussions. 2013;161:31-43.
[52] Sanchez SA, Tricerri MA, Gratton E. Laurdan generalized polarization fluctuations measures membrane packing micro-heterogeneity in vivo. Proceedings of the National Academy of Sciences. 2012;109:7314-9.
[53] Sezgin E, Waithe D, Bernardino de la Serna J, Eggeling C. Spectral Imaging to Measure Heterogeneity in Membrane Lipid Packing. ChemPhysChem. 2015;16:1387-94.
[54] Parasassi T, De Stasio G, d'Ubaldo A, Gratton E. Phase fluctuation in phospholipid membranes revealed by Laurdan fluorescence. Biophysical journal. 1990;57:1179.

[55] Marchi-Artzner V, Gulik-Krzywicki T, Guedeau-Boudeville MA, Gosse C, Sanderson JM, Dedieu JC, et al. Selective Adhesion, Lipid Exchange and Membrane-Fusion Processes between Vesicles of Various Sizes Bearing Complementary Molecular Recognition Groups. ChemPhysChem. 2001;2:367-76.
[56] De Cock I, Lajoinie G, Versluis M, De Smedt SC, Lentacker I. Sonoprinting and the importance of microbubble loading for the ultrasound mediated cellular delivery of nanoparticles. Biomaterials. 2016;83:294-307.
[57] Lehtonen J, Kinnunen P. Poly (ethylene glycol)-induced and temperature-dependent phase separation in fluid binary phospholipid membranes. Biophysical journal. 1995;68:525.
[58] Borden MA, Pu G, Runner GJ, Longo ML. Surface phase behavior and microstructure of lipid/PEG-emulsifier monolayer-coated microbubbles. Colloids and Surfaces B: Biointerfaces. 2004;35:209-23.
[59] Watanabe H, Kobayashi A, Yamamoto T, Suzuki S, Hayashi H, Yamazaki N. Alterations of human erythrocyte membrane fluidity by oxygen-derived free radicals and calcium. Free Radical Biology and Medicine. 1990;8:507-14.
[60] Szachowicz-Petelska B, Dobrzynska I, Sulkowski S, Figaszewski Z. Characterization of the cell membrane during cancer transformation. 2010.
[61] Harris FM, Best KB, Bell JD. Use of laurdan fluorescence intensity and polarization to distinguish between changes in membrane fluidity and phospholipid order. Bba-Biomembranes. 2002;1565:123-8.
[62] Parasassi T, De Stasio G, Ravagnan G, Rusch RM, Gratton E. Quantitation of Lipid Phases in Phospholipid-Vesicles by the Generalized Polarization of Laurdan Fluorescence. Biophysical Journal. 1991;60:179-89.
[63] Koynova R, Caffrey M. Phases and phase transitions of the phosphatidylcholines (vol 1376, pg 91, 1998). Bba-Biomembranes. 2001;1513:82-.
[64] Longo M, Lozano M, Borden M. Physical chemistry of experimental models for lipid shells of medical microbubbles. Bubble Science, Engineering & Technology. 2009;1:18-30.
[65] Yamaguchi T, Masato K, FUJITA Y, KIMOTO E. Effects of pH on membrane fluidity of human erythrocytes. Journal of biochemistry. 1982;91:1299-304.
[66] Ohno H, Sakai T, Tsuchida E, Honda K, Sasakawa S. Interaction of human erythrocyte ghosts or liposomes with polyethylene glycol detected by fluorescence polarization. Biochemical and biophysical research communications. 1981;102:426-31.
[67] Butler PJ, Norwich G, Weinbaum S, Chien S. Shear stress induces a time-and position-dependent increase in endothelial cell membrane fluidity. American Journal of Physiology-Cell Physiology. 2001;280:C962-C9.
[68] Haidekker MA, L'Heureux N, Frangos JA. Fluid shear stress increases membrane fluidity in endothelial cells: a study with DCVJ fluorescence. American Journal of Physiology-Heart and Circulatory Physiology. 2000;278:H1401-H6.
[69] Li Y-SJ, Haga JH, Chien S. Molecular basis of the effects of shear stress on vascular endothelial cells. Journal of biomechanics. 2005;38:1949-71.
[70] Chen X, Leow RS, Hu Y, Wan JM, Alfred C. Single-site sonoporation disrupts actin cytoskeleton organization. Journal of The Royal Society Interface. 2014;11:20140071.

[71] Tran TA, Le Guennec JY, Bougnoux P, Tranquart F, Bouakaz A. Characterization of cell membrane response to ultrasound activated microbubbles. Ultrasonics, Ferroelectrics, and Frequency Control, IEEE Transactions on. 2008;55:43-9.
[72] Kumon RE, Aehle M, Sabens D, Parikh P, Han Y, Kourennyi D, et al. Spatiotemporal effects of sonoporation measured by real-time calcium imaging. Ultrasound in medicine & biology. 2009;35:494-506.
[73] Fokong S, Theek B, Wu Z, Koczera P, Appold L, Jorge S, et al. Image-guided, targeted and triggered drug delivery to tumors using polymer-based microbubbles. Journal of controlled release. 2012;163:75-81.
[74] Sutton JT, Haworth KJ, Pyne-Geithman G, Holland CK. Ultrasound-mediated drug delivery for cardiovascular disease. Expert opinion on drug delivery. 2013;10:573-92.
[75] Schneider M, Arditi M, Barrau M-B, Brochot J, Broillet A, Ventrone R, et al. BR1: a new ultrasonographic contrast agent based on sulfur hexafluoride-filled microbubbles. Investigative radiology. 1995;30:451-7.
[76] Brancewicz C, Rasmussen DH, Papahadjopoulos-Sternberg B. Hydrophobic gas bubble formation in Definity®: A freeze fracture electron microscopy study. Journal of dispersion science and technology. 2006;27:761-5.

Figure Captions

Fig. 1. Microbubble sizing. (A) Bright-field microscope image of DSPC-PEG40S (9:1 molar ratio) MBs produced by sonication, and (B) corresponding size distribution. (C) Fluorescent confocal microscope image of DiI labelled MBs demonstrating dye incorporation within the MB shell, and (D) size distribution of DiI labelled microbubbles. Size distributions in all cases were determined from bright field microscope images using a purpose built MATLAB routine.

Fig. 2. Design and construction of acoustofluidic devices. (A) Photograph of the assembled device positioned on a microscope stage. (B) Expanded view of the individual layers of the device. (C) Normalised acoustic pressure through the layers of the device, obtained from 1-D transfer impedance modelling, showing minimal pressure gradient across the fluid layer thickness.

Fig. 3. Summary of the generalized polarization (GP) image processing for A 594 cells. (A-B) 440 nm and 490 nm wavelength emission greyscale images following Otsu's method thresholding, (C) pseudo-coloured GP map of the same cell, and (D) the GP map used for analysis following membrane segmentation. C-Laurdan GP ranges from -1 to 1, where greater GP indicates greater lipid order.

Fig. 4. Observations of the transfer of DiI from microbubbles to cells by fluorescence microscopy. Panels A-F: representative composite images of transfer from DiI-loaded DSPC-PEG40S, DSPC, and DBPC MBs (DiI, green) to A-549 cells (CellMask, red), with and without US. Panels A, B, D, and E were acquired with a 20x microscope objective and panels C and F were acquired with a 63x objective. The scale bar applies for all images. Panel G: three-dimensional map of colocalization of DiI and CellMask from a confocal z-stack (1 μm slice thickness) of the same cells in Panel C (indicated by white arrows). The color bar indicates distance from the substrate in microns.

Fig. 5. Changes in the physical properties of DOPC GUVs exposed to US (US) and MBs (MB). (A) Lifetime (in ns) of BODIPY-C_{12} rotor in DOPC GUVs exposed to a PBS sham (control), US (US), and DSPC-PEG40S MBs with and without US respectively. (B) C-Laurdan generalised polarisation (GP) in DOPC GUVs exposed to a PBS sham (control), US (US), and DSPC-PEG40S MBs with and without US respectively. (C) Diffusion time (τ_D, in ms) of cholesterol-PEG-KK114 in DOPC GUVs exposed to a PBS sham (control), US (US), and DSPC-PEG40S MBs with and without US respectively. Bars and error bars indicate mean ± standard deviation ΔGP. The asterisk (*) indicates statistical significance ($p < 0.01$) as compared to the control.

Fig. 6. Representative pseudo-coloured membrane generalized polarization (GP) maps of A-549 cell membranes before (top) and after (bottom) exposure to a PBS sham (control), US (US), and DSPC or DSPC-PEG40S MBs with and without US respectively. The change in GP ($\Delta GP = GP_{after} - GP_{before}$) for each representative specimen is reported below its corresponding membrane GP map.

Fig. 7. Effects of DSPC-PEG40S molar ratio on C-Laurdan generalized polarization (ΔGP) in A-549 cell membranes. A-549 cells were exposed to a PBS sham (control), and MB with DSPC-PEG40S molar ratios of 9:1 (with and without washing by centrifugation), 90:1, and 1:0 (DSPC only), with and without US. Cells were also exposed to sonicated PEG40S (0:1 molar ratio). $\Delta GP < 0$ or $\Delta GP > 0$ signify a decrease or increase in membrane lipid order, respectively. Over the course of 3 independent experiments per condition, 373 cell membranes were analyzed before and after exposure. Bars and error bars indicate mean ± standard deviation ΔGP. The asterisk (*) indicates statistical significance ($p < 0.01$) as compared to the control.

Fig. 8. Effects of MB of different lipid chain lengths on C-Laurdan generalized polarization (ΔGP) in A-549 cell membranes. A-549 cells were exposed to a PBS sham (control), DSPC MB (18:0 PC), and DBPC MB (22:0 PC) with and without US. Over the course of 3 independent experiments per condition, 258 cell membranes were analyzed before and after exposure. Bars and error bars indicate mean ± standard deviation ΔGP. The asterisk (*) indicates statistical significance ($p < 0.01$) as compared to the control.

Fig. 9. Effects of DSPC-PEG40S 9:1 MB on C-Laurdan generalized polarization (ΔGP) in A-549 and CHO-K1 cell membranes. A-549 and CHO-K1 cells were exposed to a PBS sham (control), US, MB, and MB with US. Over the course of 3 independent experiments per condition, 156 A-549 cell membranes and 225 CHO-K1 cell membranes were analyzed before and after exposure. Bars and error bars indicate mean ± standard deviation ΔGP. The asterisk (*) indicates statistical significance ($p < 0.01$) as compared to the respective controls for each cell line.

Figure 1

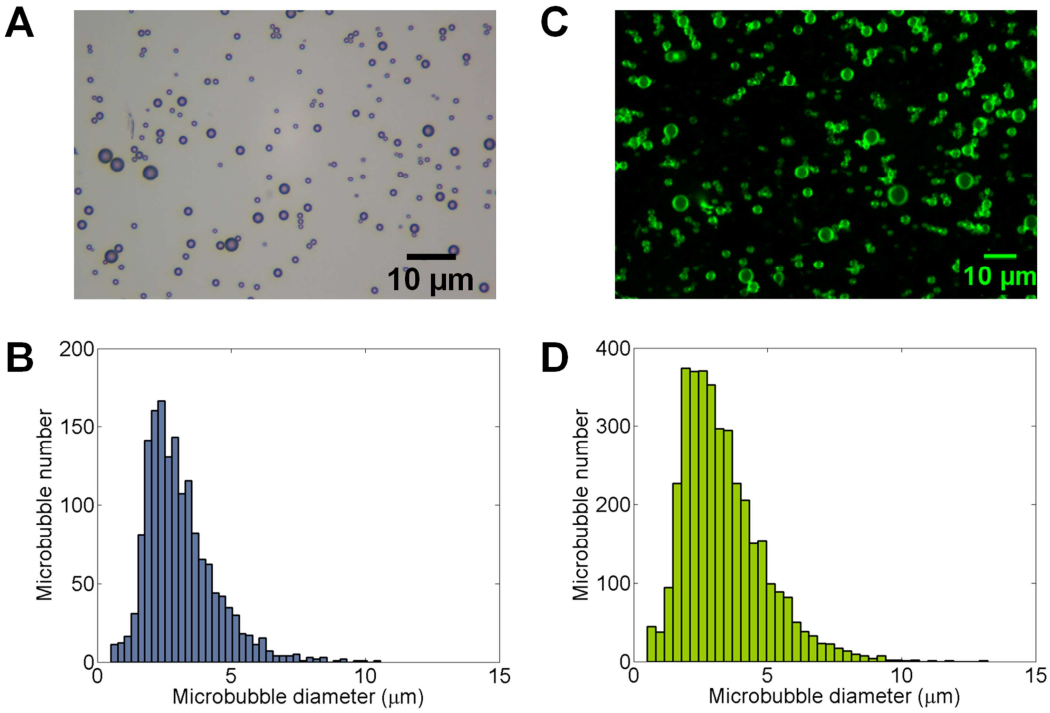

Figure 2

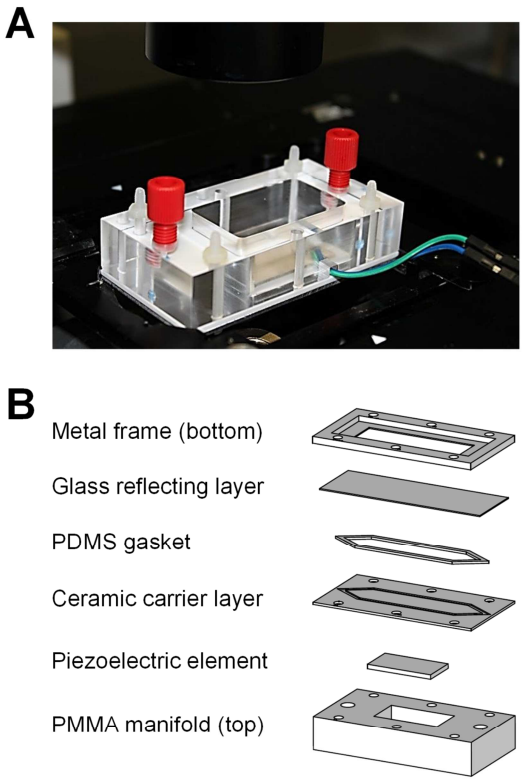
A
B
Metal frame (bottom)
Glass reflecting layer
PDMS gasket
Ceramic carrier layer
Piezoelectric element
PMMA manifold (top)
C
Normalized acoustic pressure (Pa/Pa)
Distance through device layers (mm)
Matching layer
Fluid layer
Reflecting layer
0
0.2
0.4
0.6
0.8
1
0.5
1.5
2

Figure 3

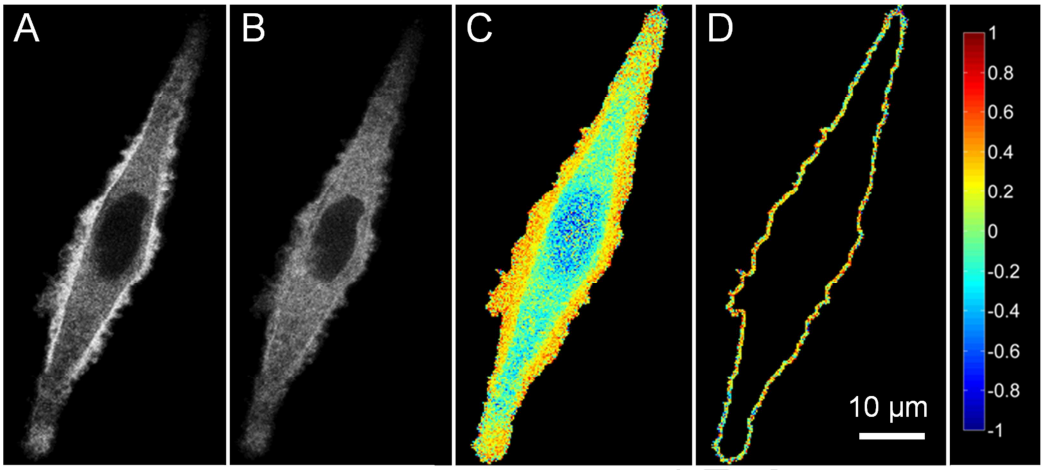

Figure 4

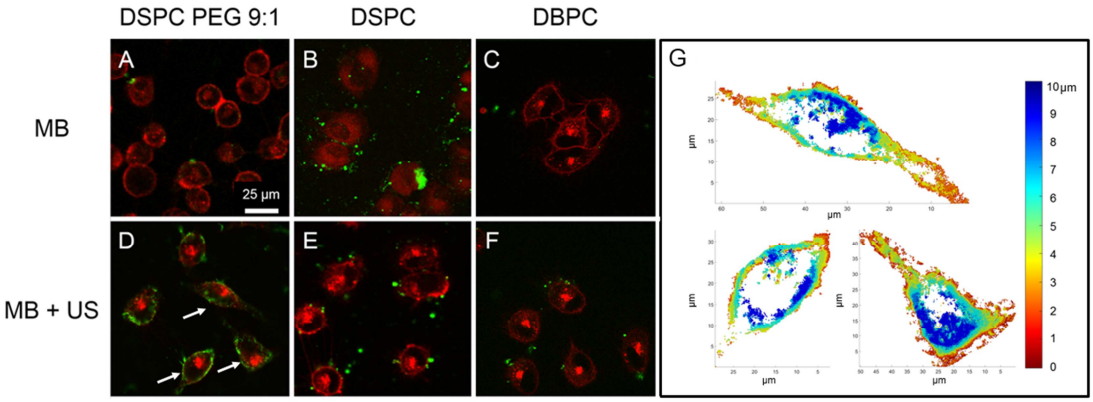

Figure 5

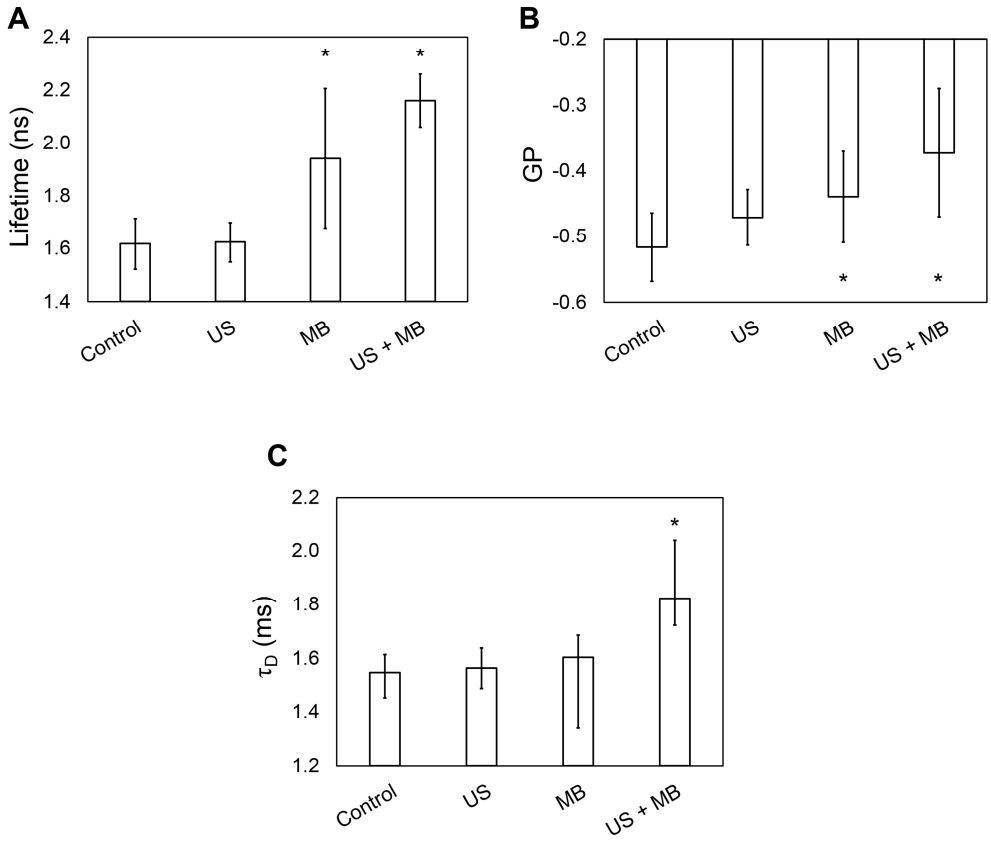

Figure 6

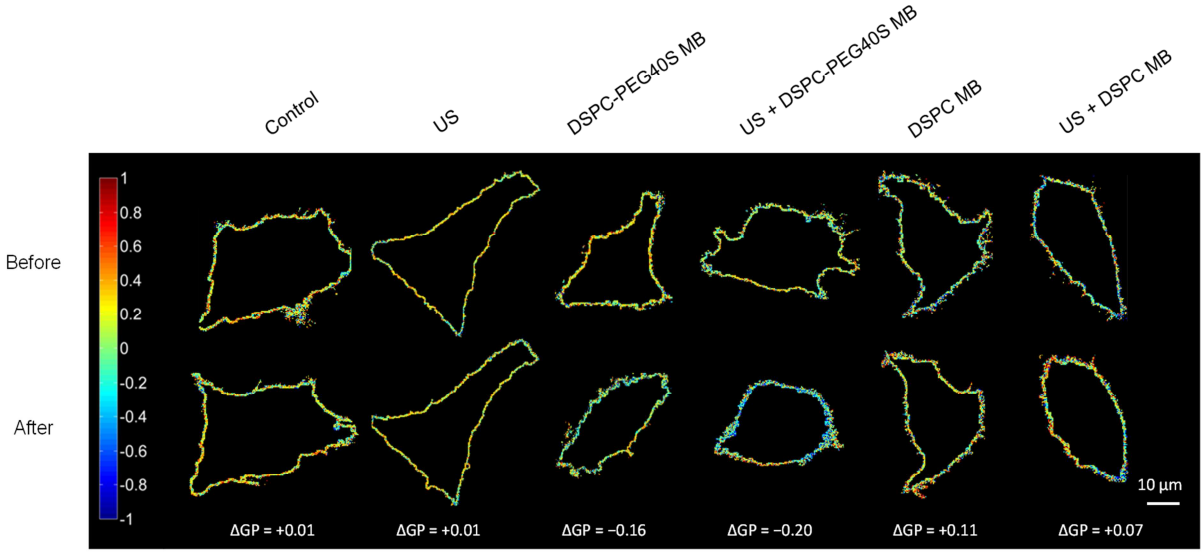

Figure 7

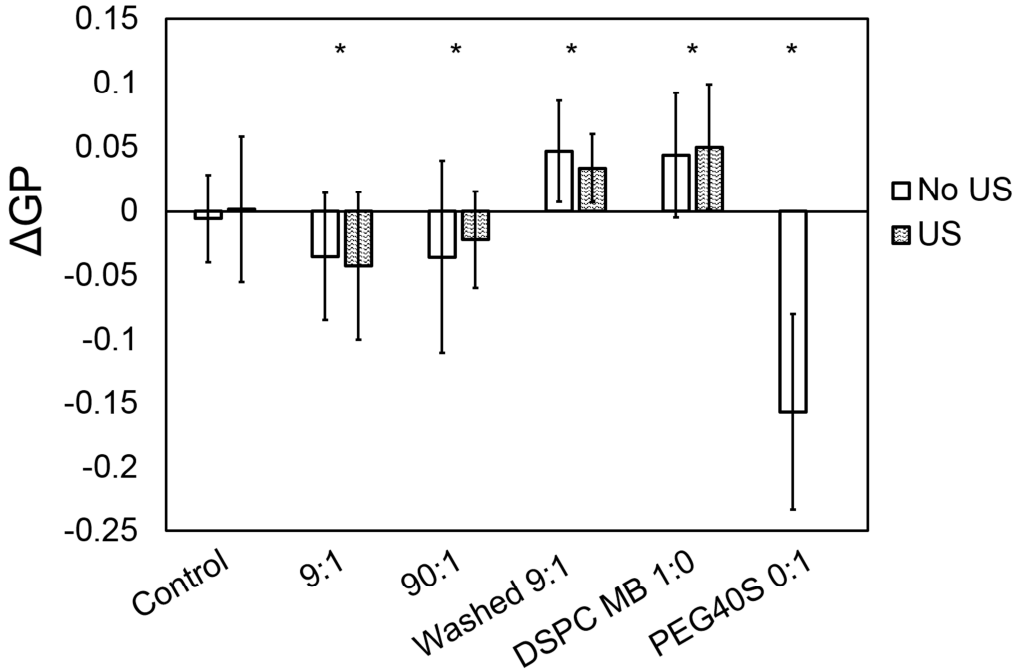

Figure 8

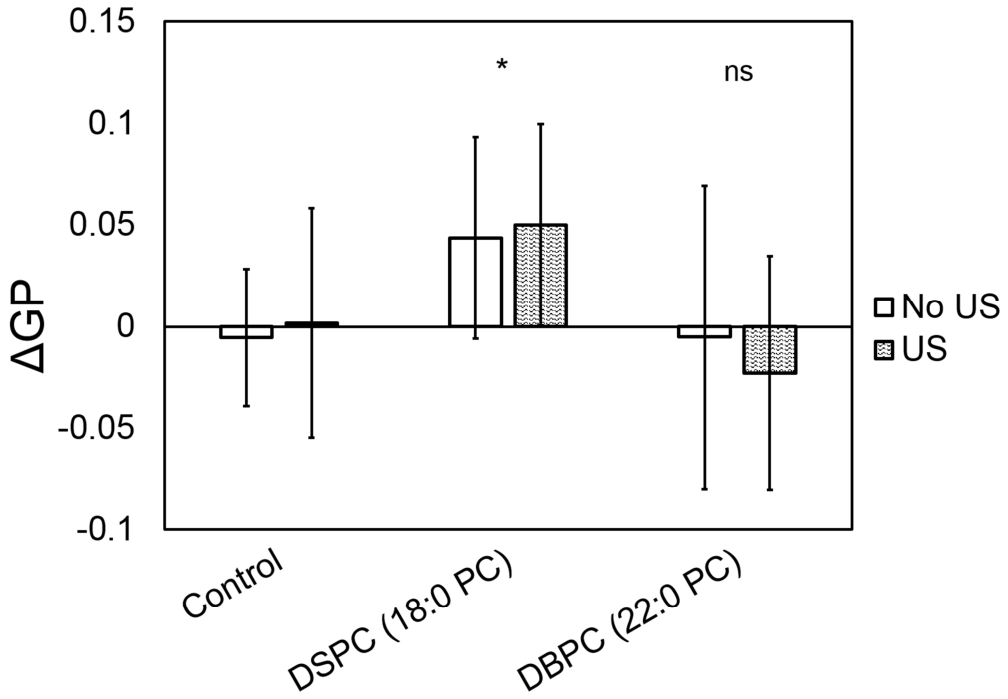

Figure 9

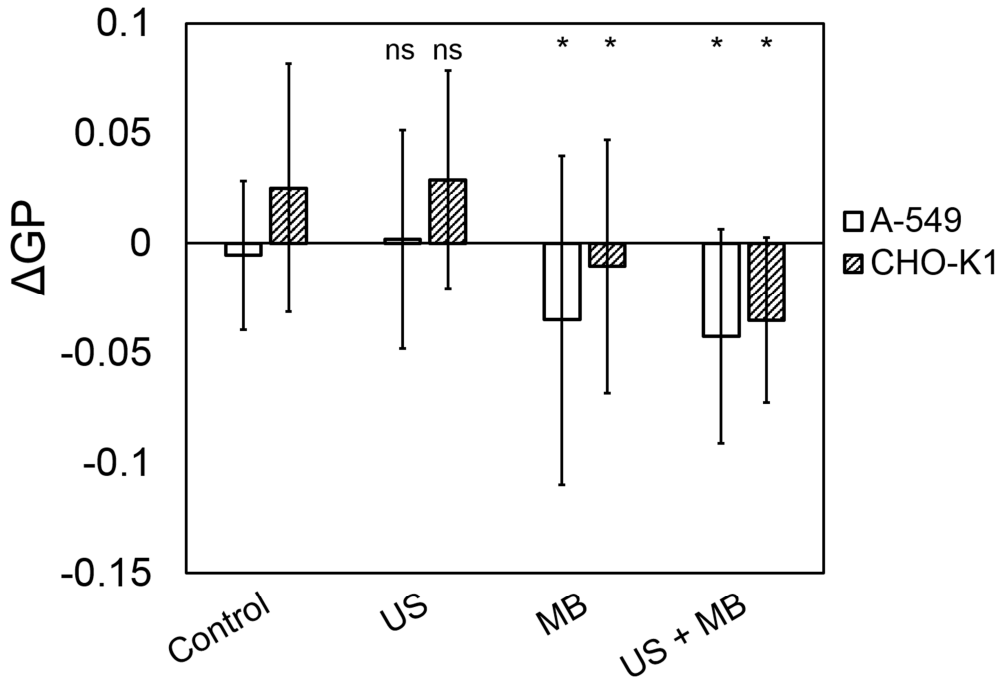

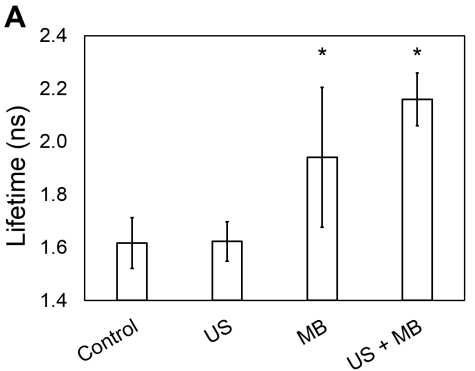
A
Lifetime (ns)
2.4
2.2
2.0
1.8
1.6
1.4
*
*
Control
US
MB
US + MB

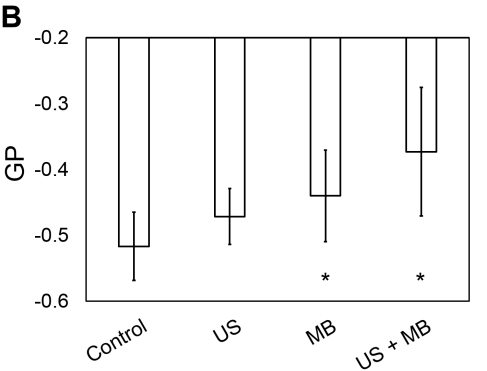
B
GP
-0.2
-0.3
-0.4
-0.5
-0.6
*
*
Control
US
MB
US + MB

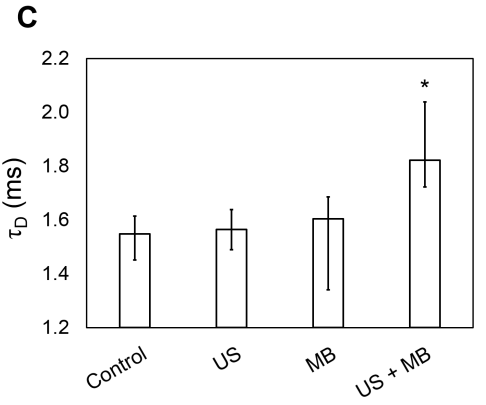
C
τD (ms)
2.2
2.0
1.8
1.6
1.4
1.2
*
Control
US
MB
US + MB